8-30-2011

Control of an indoor autonomous mobile communications relay via antenna diversity

Brian Griffin

Brian M. Griffin
Candidate

Electrical and Computer Engineering
Department

This thesis is approved, and it is acceptable in quality and form for publication:

Approved by the Thesis Committee:

,Chairperson

Control of an Indoor Autonomous Mobile Communications Relay via Antenna Diversity

by

Brian M. Griffin

B.E., Mechanical Engineering, Auburn University, 2004

THESIS

Submitted in Partial Fulfillment of the

Requirements for the Degree of

Master of Science

Electrical Engineering

The University of New Mexico

Albuquerque, New Mexico

July, 2011

Dedication

To my wife, Sarah, for her love and support.

Acknowledgments

I would like to thank my advisor, Professor Rafael Fierro, for his help as well as his patience. I would also like to thank Professor Chaouki Abdallah and Professor Sudharman Jayaweera for serving as members on my committee.

Control of an Indoor Autonomous Mobile Communications Relay via Antenna Diversity

by

Brian M. Griffin

ABSTRACT OF THESIS

Submitted in Partial Fulfillment of the
Requirements for the Degree of

Master of Science
Electrical Engineering

The University of New Mexico

Albuquerque, New Mexico

July, 2011

Control of an Indoor Autonomous Mobile Communications Relay via Antenna Diversity

by

Brian M. Griffin

B.E., Mechanical Engineering, Auburn University, 2004

M.S., Electrical Engineering, University of New Mexico, 2011

Abstract

Presented in this thesis is a motion planning scheme for enabling a quadrotor unmanned aerial vehicle (UAV) to serve as an autonomous communications relay in indoor or GPS-denied environments. The goal of the algorithm is to maximize the throughput of the end-to-end communications channel. An extremum-seeking controller steers the quadrotor while collision avoidance is provided by artificial potential fields.

Extremum-seeking is model-free adaptive control method; it's applicable in situations where there is a nonlinearity in the control problem and the nonlinearity has a local minimum or maximum. The extremum-seeking controller presented here is driven by antenna diversity and attempts to optimize the inputs to an unknown, time-varying cost function characterized by the RF environment. Each of the multiple antennas onboard the quadrotor receives the same incoming packets and provides

associated signal strength measurements. The extremum-seeking controller then uses these measurements to autonomously fly the quadrotor communications relay to an optimal location so as to maximize throughput, all without positioning data.

This work is motivated by the need to extend the operating ranges of robots in complex urban and indoor environments. The algorithm and necessary technical background are presented in detail. Simulations results verify the validity of the proposed extremum-seeking approach. Experiments demonstrate the feasability of implementing the extremum-seeking controller with tangible hardware.

Contents

List of Figures

List of Tables

Glossary

γ	Signal path loss exponent.
$\delta = \{1, -1\}$	Orientation vector for G_b.
ϵ	Dither size (i.e., length between quadrotor center of mass and antenna).
λ	Signal wavelength.
τ	Total torque acting about the quadrotor's center of mass.
$\begin{bmatrix}\phi & \theta & \psi\end{bmatrix}$	Quadrotor roll, pitch, yaw euler angles.
$\boldsymbol{\omega} = \begin{bmatrix}p & q & r\end{bmatrix}$	Quadrotor body angular velocities.
$\Omega_i,\ i = 1:4$	Angular speed of each of the quadrotor's motors.
C	Channel capacity, in bits per second.
b	Thrust coefficient.
B	Bandwidth, in hertz.
d	Drag coefficient.
d	Distance between transmitter and receiver.

Glossary

d_0	Reference distance between transmitter and receiver.
$D(x)$	Distance between quadrotor sensor and object.
D^*	Range of collision avoidance sensor.
e_i, e_j	ith and jth unit vectors.
F	Total force acting on the quadrotor's center of mass.
$F_i,\ i = 1:4$	Force produced by each of the quadrotor's propellers.
$F(x, y)$	Smooth function characterizing RF field.
g	Gravity.
G_b	Balancing gradient.
G_{ca}	Collision avoidance gradient.
G_p	Peak-seeking gradient.
G_{Rx}	Receive antenna gain.
G_{Tx}	Transmit antenna gain.
$I = \begin{bmatrix} I_x & I_y & I_z \end{bmatrix}$	Moment of inertia about the center of mass.
I_3	3-by-3 identity matrix.
J_R	Rotor inertia.
K_b	Gain associated with balancing gradient.
K_{ca}	Gain associated with collision avoidance gradient.
K_p	Gain associated with peak-seeking gradient.

Glossary

L	Distance between quadrotor's center of mass and its motors.
m	Quadrotor's mass.
$M_i,\ i = 1:4$	Moment produced by each of the quadrotor's propellers.
P_{noise}	Average power of background noise, in dBm.
P_{Rx}	Receive power, in dBm.
P_{signal}	Average power of signal, in dBm.
P_{Tx}	Transmit power, in dBm.
PL	Path loss, in dB.
PL_0	Path loss at reference distance, d_0, in dB.
R	Rotation matrix.
$\frac{S}{N}$	Signal-to-noise ratio (SNR).
$\mathbf{x} = \begin{bmatrix} x & y \end{bmatrix}$	Quadrotor position in horizontal plane (point-mass representation).
$\mathbf{x_W} = \begin{bmatrix} x_W & y_W & z_W \end{bmatrix}$	Quadrotor position in world/inertial coordinate frame (center of mass representation).
$\mathbf{x_B} = \begin{bmatrix} x_B & y_B & z_B \end{bmatrix}$	Quadrotor position in body-fixed coordinate frame (center of mass representation).

Chapter 1

Introduction

1.1 Motivation

In modern-day warfare, the most likely battlefield is an urban environment. Superior militaries control the skies and ground so hostile forces resort to fighting from inside buildings, traveling through tunnels and sewers, and hiding in caves. Having soldiers search and clear these areas is extremely dangerous due to the possible presence of booby traps or waiting enemies [1]. Unmanned ground vehicles (UGVs) have become a desired asset for the military as they can perform such missions while keeping personnel out of harm's way.

One such mobile robot is the Small Unmanned Ground Vehicle (SUGV) developed by iRobot Boeing. Shown in Figure 1.1 entering a building, the SUGV is a lightweight, man-portable mobile robot which can be thrown into a room or cave. The SUGV can climb stairs or move over rubble and bad terrain in all weather conditions while streaming video and audio back to an operator. The robot can be equipped with a dexterous manipulator as well as a variety of sensors including electroptical and infrared cameras and chemical, biological, and radiation sensors [2].

Figure 1.1: iRobot SUGV.

Whether it's the military missions discussed above, police forces disarming or disposing of a bomb, or first-responders performing hazardous material detection or search and rescue amongst wreckage in a disaster area, mobile robots such as the SUGV are typically controlled from a ground station external to the environment. A considerable weakness of these robots is the communications link back to the operator. These links may be hardwired but cable tethers are cumbersome, limit manueverability, and are susceptible to snagging and breaking. High-frequency digital communications are the preferred means for maintaining connectivity between the robot and ground station due to the high bandwidth available for transmitting data and imagery. These radio frequency (RF) signals, however, are susceptible to interference, multipath, and attenuation, making communication difficult to maintain in indoor or urban environments. As a UGV descends further into a building, tunnel, or cave, the communications link back to the operator degrades and the robots are thus limited to line-of-sight (LOS) operations.

The problem can be alleviated to a certain extent by higher power transmissions and spread spectrum techniques (i.e., frequency hopping), but the use of these is limited by size, weight, battery life, and spectrum availability. An alternative and

arguably better way of solving this problem is to add communications relays between the ground station and robot, creating a communications chain where the relay nodes provide a series of LOS and near LOS of links. The quality of the end-to-end wireless communication link is directly influenced by the location of the nodes in the radio propogation network. While the end nodes (e.g., the UGV and ground station in the scenario presented here) may move independently, the relay nodes should be positioned so as to improve the throughput of the communications chain. For this reason, mobile relays nodes are preferable to static nodes as they can autonomously move in order to optimize their respective links.

1.2 Prior Work

The authors in [3] were the first to propose using controlled mobility for improving the communications performance of a network of mobile agents. The proposed scenario consists of fixed source and destination nodes with some number of mobile relay nodes whereby each agent know its position and the position of its neighbors and attempts to optimize the communications chain based on this information. Execution of the algorithm results in the nodes assuming a position on the straight line between the source and destination nodes with equidistant spacing between each node. As this approach does not take into account any actual measure of the quality of the communications links, the resultant throughput will likely be less than optimal, especially in the presence of noise sources and physical obstructions.

1.2.1 UAV Communications Relay

Several existing military UAVs have in recent years taken on the additional role of serving as a communications relay as they're capable of providing more band-

width and less latency than satellite communications. This includes large fixed-wing UAVs such as Northrop Grumman's Global Hawk, General Atomics's Predator, and AAI's Shadow and the unmanned helicopter, Northrop Grumman's Fire Scout [4]. These systems typically use the Global Positioning System (GPS) and multiple radios to provide battlefield coverage such as relaying ground-to-ground communications around mountainous terrain.

Most research to date has focused on position-based solutions. In [5], the author employed mixed integer linear programming (MILP) in order to position one or multiple rotorcraft UAVs between a user-controlled helicopter and the accompanying ground station. The relay nodes are located so as to maintain LOS links with its neighboring nodes. The authors in [6] attempted to solve the same problem but by using a Bellman-Ford algorithm.

In [7, 8], the authors moved beyond the traditional position-based methods in order to intelligently locate a fixed-wing UAV that serves as a relay node in a communications chain. As a fixed-wing UAV has to maintain continual forward motion in order to stay aloft, the researchers used this to their advantage. The aircraft is commanded to continually orbit around a center-point (i.e., a one-waypoint flight plan). As it circles, signal-to-noise ratio (SNR) measurements are taken so as to estimate the gradient of the communications field. The location of the UAV's orbit center-point is then moved based on the gradient field constructed by these SNR measurements in order to improve the quality of the end-to-end communications link.

Similarly, the authors in [9] used quadrotor UAVs as communications relays to provide connectivity between a group of ground robots. Vehicle positions, obtained from GPS, are shared between all of the UAVs and UGVs. Signal-to-Interference Ratio (SIR) measurements are taken by each UAV for each of its communications links. The positioning information and SIR measurements are then used as inputs

Figure 1.2: Conceptual LANdroid.

into a cost function — the negative gradient of the cost function is used to independently drive each UAV to an optimal position where they can provide communication coverage while maintaining seperation between themselves and the other relay UAVs.

1.2.2 Indoor Communications Relay

Little work has been done regarding the use of communications relays in indoor or GPS-denied environments. The United States Department of Defense is addressing this void by way of the Defense Advanced Research Projects Agency (DARPA) LANdroids program. The goal of LANdroids is to create intelligent, autonomous radio relay UGVs that maintain communication networks in urban settings. The ideal LANdroid robot will be pocket-sized, inexpensive, and expendable — a notional landroid is shown in Figure 1.2. Ideally, a user will carry multiple LANdroids and deploy them as needed and the robots will self-organize so as to maintain the communications network [10].

Similar research is being conducted by Space and Naval War Systems Command

Figure 1.3: SPAWAR AMCR and ADCR.

(SPAWAR). The goal of SPAWAR's research is to extend a robot's operating range when operating in non-line-of-sight (NLOS) environments. The Autonomous Mobile Communications Relay (AMCR) system consists of an operator-controlled reconnaissance robot with multiple slave robots convoying behind the lead. As the communications link drops below a specified threshold, individual robots stop and function as static relay nodes. The mobility of the relay nodes allows the robots to catch up to the lead robot when no longer needed [11, 12]. SPAWAR has also developed the more practical and cost-effective Automatically Deployed Communications Relay (ADCR) system. The lead robot in this system deploys static radio repeaters shaped like bricks which right themselves and extend their antennas when dropped off. Without mobility, however, there is no means for automatic recovery of relay bricks [13][14].

1.3 Problem Statement

As a teleoperated robot descends deeper into the interior of a building, the communications link can degrade rapidly. Indoor communications are susceptible to severe

multipath and large propogation losses – a deep fade at a given frequency in an indoor channel can last for several seconds, or even minutes [15]. This issue can be resolved by adding relay nodes between the robot and the ground station. The goal of the research presented in this thesis is to provide a means for moving and locating a communications relay in an indoor environment where independent positioning information (e.g., GPS, motion capture systems) is unavailable. The relay robot maintains strong RF links without operator intervention or knowledge.

The chosen communications relay platform is a quadrotor UAV — the reasoning for this is discussed in Chapter 2. The proposed method utilizes antenna diversity as the input into an extremum-seeking algorithm as will be explained in Chapter 4. It is believed this is the first work to present the concept of using UAVs as indoor communications relays.

In the scenario depicted in Figure 1.4, a quadrotor UAV serves as a communications relay for a ground robot in a disaster area. While the ground station to UGV scenario is the motivation for this research, the algorithm presented here may be applicable to any situation where a communications relay is needed.

1.4 Organization of Thesis

The remainder of this thesis is organized as follows. Chapter 2 provides background information on quadrotors and presents the quadrotor model and low-level control. Chapter 4 introduces the concepts of antenna diversity and extremum-seeking algorithms before presenting the proposed high-level controller for an autonomous communications relay. Simulations of the algorithm follow in Chapter 5 and hardware experimentation results are contained in Chapter 6. Chapter 7 discusses conclusions and potential future work.

Figure 1.4: Communications relay scenario.

Chapter 2

Quadrotors

2.1 Quadrotor Basics

As its name suggests, a quadrotor is propelled by four rotors — two spinning clockwise and two spinning counter-clockwise. Quadrotors can hover, ascend, or descend by increasing/decreasing all four motor speeds together. Changing either the clockwise or counter-clockwise rotor pairs inversely proportional to each other allows the quadrotor to move laterally in any direction (pitch and roll) while maintaing a constant heading. Conversely, changing the rotor pairs relative to eachother (e.g., uniformly increasing speed of counter-clockwise rotors while decreasing speed of counter-clockwise rotors) allows the quadrotor to rotate (i.e., yaw) about its vertical axis. Manipulating the four fixed-pitch rotors, therefore, allows the quadrotor to move in any direction.

Quadrotors are highly nonlinear mechanical systems, similar to a helicopter but smaller in size and less complex as there's no variable pitch rotor blade. The simplistic hardware design makes quadrotors very robust — a desired asset for flying indoors where crashes, at least during experimentation, are inevitable. The ability

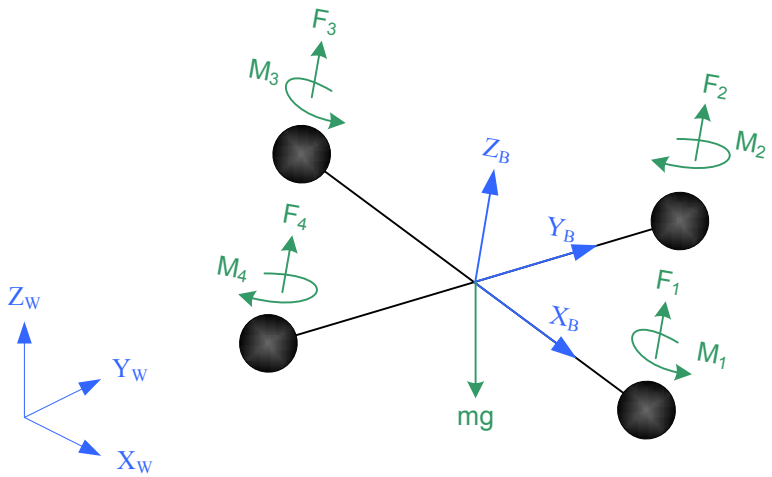

Figure 2.1: Quadrotor coordinate system and free body diagram.

to hover and fly in highly constrained spaces provides significant advantages over fixed-wing UAVs and similarly, the ability to fly above, below, and around obstacles allows a quadrotor to function in an environment where a UGV may be stalled. The manuverability, robustness, and diminutive size makes a quadrotor UAV an ideal platform for an indoor communications relay.

2.2 Quadrotor Model

The quadrotor is modeled as a single rigid body in a flat, stationary earth. Figure 2.1 shows the coordinate system and free body diagram for modeling the quadrotor dynamics [16, 17, 18]. The inertial frame (i.e., world frame), W, is defined by axes x_W, y_W, and z_W, where z_W is positive up. The body-fixed coordinate frame, B, coincides with the center of mass of the quadrotor and is defined by axes x_B, y_B, and z_B. The quadrotor's centor of mass in the inertial frame is specified by the position vector $\mathbf{x} = \begin{bmatrix} x_W & y_W & z_W \end{bmatrix}^T$. The roll, pitch, and yaw Euler angles, ϕ, θ, and ψ, specify the quadrotor's attitude and the body angular velocitiy is then defined as

the rate vector $\boldsymbol{\omega} = \begin{bmatrix} p & q & r \end{bmatrix}^T$. The rotation matrix, R, consists of succesive Z-X-Y rotations and is used to transform coordinates from B to W.

$$
\begin{aligned}
R &= R_z(\psi)R_x(\phi)R_y(\theta) \qquad (2.1)\\
&= \begin{bmatrix} \cos\psi & -\sin\psi & 0 \\ \sin\psi & \cos\psi & 0 \\ 0 & 0 & 1 \end{bmatrix} \begin{bmatrix} 1 & 0 & 0 \\ 0 & \cos\phi & -\sin\phi \\ 0 & \sin\phi & \cos\phi \end{bmatrix} \begin{bmatrix} \cos\theta & 0 & \sin\theta \\ 0 & 1 & 0 \\ -\sin\theta & 0 & \cos\theta \end{bmatrix} \\
&= \begin{bmatrix} \cos\psi\cos\theta - \sin\psi\sin\phi\sin\theta & -\sin\psi\cos\phi & \cos\psi\sin\theta + \sin\psi\sin\phi\cos\theta \\ \cos\psi\sin\phi\sin\theta + \sin\psi\cos\theta & \cos\psi\cos\phi & \sin\psi\sin\theta - \cos\psi\sin\phi\cos\theta \\ -\cos\phi\sin\theta & \sin\phi & \cos\phi\cos\theta \end{bmatrix}
\end{aligned}
$$

The time derivative of the Euler angles can be calculated directly from the body rates which are measured onboard the quadrotor by gyroscopes[19]. Resolving the rate of change of the Euler angles into the body-fixed coordinate frame results in the following relationship.

$$
\begin{aligned}
\begin{bmatrix} p \\ q \\ r \end{bmatrix} &= R_y(\theta)^T R_x(\phi)^T \begin{bmatrix} 0 \\ 0 \\ \dot{\psi} \end{bmatrix} + R_y(\theta)^T \begin{bmatrix} \dot{\phi} \\ 0 \\ 0 \end{bmatrix} + \begin{bmatrix} 0 \\ \dot{\theta} \\ 0 \end{bmatrix} \\
&= \begin{bmatrix} \cos\theta & 0 & -\sin\theta \\ 0 & 1 & 0 \\ \sin\theta & 0 & \cos\theta \end{bmatrix} \begin{bmatrix} 1 & 0 & 0 \\ 0 & \cos\phi & \sin\phi \\ 0 & -\sin\phi & \cos\phi \end{bmatrix} \begin{bmatrix} 0 \\ 0 \\ \dot{\psi} \end{bmatrix} \\
&\quad + \begin{bmatrix} \cos\theta & 0 & -\sin\theta \\ 0 & 1 & 0 \\ \sin\theta & 0 & \cos\theta \end{bmatrix} \begin{bmatrix} \dot{\phi} \\ 0 \\ 0 \end{bmatrix} + \begin{bmatrix} 0 \\ \dot{\theta} \\ 0 \end{bmatrix} \\
&= \begin{bmatrix} \cos\theta & 0 & -\sin\theta\cos\phi \\ 0 & 1 & \sin\phi \\ \sin\theta & 0 & \cos\theta\cos\phi \end{bmatrix} \begin{bmatrix} \dot{\phi} \\ \dot{\theta} \\ \dot{\psi} \end{bmatrix} \qquad (2.2)
\end{aligned}
$$

Inverting the matrix in Equation 2.2 provides the desired relationship between the body rate vector and the Euler rate vector.

$$\begin{bmatrix} \dot{\phi} \\ \dot{\theta} \\ \dot{\psi} \end{bmatrix} = \begin{bmatrix} \cos\theta & 0 & \sin\theta \\ \sin\theta\tan\phi & 1 & -\cos\theta\tan\phi \\ \frac{-\sin\theta}{\cos\phi} & 0 & \frac{\cos\theta}{\cos\phi} \end{bmatrix} \begin{bmatrix} p \\ q \\ r \end{bmatrix} \tag{2.3}$$

The quadrotor rigid body dynamics are described by the Newton-Euler equations [18].

$$\begin{bmatrix} F \\ \tau \end{bmatrix} = \begin{bmatrix} mI_3 & 0 \\ 0 & I \end{bmatrix} \begin{bmatrix} \ddot{\mathbf{x}} \\ \dot{\boldsymbol{\omega}} \end{bmatrix} + \begin{bmatrix} \boldsymbol{\omega} \times m\dot{\mathbf{x}} \\ \boldsymbol{\omega} \times I\boldsymbol{\omega} \end{bmatrix} \tag{2.4}$$

where

$F =$ total force acting on the center of mass

$\tau =$ total torque acting about the center of mass

$m =$ quadrotor mass

$I_3 =$ identity matrix of size 3-by-3

$\mathbf{x} =$ position of the center of mass

$I =$ moment of inertia about the center of mass

$\boldsymbol{\omega} =$ angular velocity of the quadrotor

The last term in the Newton equation, $\boldsymbol{\omega} \times m\dot{\mathbf{x}}$, accounts for fictitious forces (e.g., centrifugal force, coriolis effect) if a non-inertial frame of reference is used (i.e., body-fixed frame). As the forces will be summed in the world frame for the quadrotor model presented here, this term is equal to zero.

From equation 2.4, the translational dynamics describe the acceleration of the quadrotor's center of mass using the inertial frame of reference. F_i represents each

of the forces acting in the z_b direction, produced by the quadrotor's four propellers.

$$m\ddot{\mathbf{x}} = \begin{bmatrix} 0 \\ 0 \\ -mg \end{bmatrix} + R \begin{bmatrix} 0 \\ 0 \\ \sum F_i \end{bmatrix} \tag{2.5}$$

The force produced by each rotor is modeled by $F_i = b\Omega_i^2$ with Ω_i corresponding to the respecitve motor's angular speed and parameter b representing the thrust coefficient. The updated Newton equation is then as follows.

$$\begin{aligned} m\ddot{x_W} &= (\cos\psi \sin\theta + \sin\psi \sin\phi \cos\theta) b(\Omega_1^2 + \Omega_2^2 + \Omega_3^2 + \Omega_4^2) \\ m\ddot{y_W} &= (\sin\psi \sin\theta - \cos\psi \sin\phi \cos\theta) b(\Omega_1^2 + \Omega_2^2 + \Omega_3^2 + \Omega_4^2) \\ m\ddot{z_W} &= -mg + (\cos\phi \cos\theta) b(\Omega_1^2 + \Omega_2^2 + \Omega_3^2 + \Omega_4^2) \end{aligned} \tag{2.6}$$

From Equation 2.4, the rotational dynamics describe the angular acceleration of the quadrotor's center of mass using the body-fixed frame of reference. M_i represents each of the moments produced by the four propellers. The last term is added to the euler equation in order to model the gryoscopic effect resulting from the propeller rotation (spinning masses) with J_R corresponding to the rotor's inertia [17, 18].

$$I \begin{bmatrix} \dot{p} \\ \dot{q} \\ \dot{r} \end{bmatrix} = \begin{bmatrix} L(F_2 - F_4) \\ L(F_3 - F_1) \\ M_1 - M_2 + M_3 - M_4 \end{bmatrix} - \begin{bmatrix} p \\ q \\ r \end{bmatrix} \times I \begin{bmatrix} p \\ q \\ r \end{bmatrix} - \sum J_R \left(\begin{bmatrix} p \\ q \\ r \end{bmatrix} \times \begin{bmatrix} 0 \\ 0 \\ 1 \end{bmatrix} \right) \Omega_i \tag{2.7}$$

The moment produced by each rotor is modeled by $M_i = d\Omega_i^2$ with Ω_i corresponding to the respecitve motor's angular speed and parameter d representing the drag coefficient. The products of inertia are ommitted due to the symmetry of the

quadrotor. The updated Euler equation is then as follows.

$$\begin{aligned} I_x\dot{p} &= Lb(\Omega_2^2 - \Omega_4^2) - qr(I_z - I_y) - J_R q(\Omega_1 - \Omega_2 + \Omega_3 - \Omega_4) \\ I_y\dot{q} &= Lb(\Omega_3^2 - \Omega_1^2) - pr(I_x - I_z) + J_R p(\Omega_1 - \Omega_2 + \Omega_3 - \Omega_4) \\ I_z\dot{r} &= d(\Omega_1^2 - \Omega_2^2 + \Omega_3^2 - \Omega_4^2) \end{aligned} \tag{2.8}$$

2.3 Quadrotor Control

For the purpose of designing an appropriate controller, the equations of motion for the quadrotor model are linearized around the nominal hover conditions. Let the cumulative rotors inputs be defined as follows.

$$\begin{aligned} u_{collective} &= b(\Omega_1^2 + \Omega_2^2 + \Omega_3^2 + \Omega_4^2) \\ u_{roll} &= b(\Omega_2^2 - \Omega_4^2) \\ u_{pitch} &= b(\Omega_3^2 - \Omega_1^2) \\ u_{yaw} &= d(\Omega_1^2 - \Omega_2^2 + \Omega_3^2 - \Omega_4^2) \end{aligned} \tag{2.9}$$

Hover flight is characterized by small roll and pitch angles ($\cos\phi \approx \cos\theta \approx 1, \sin\phi \approx \phi, \sin\theta \approx \theta$ with euler rates approximately equal to body rates ($p = \dot{\phi}, q = \dot{\theta}, r = \dot{\psi}$). The initial quadrotor hover position is $\mathbf{x} = \mathbf{x_0}$ with heading $\psi = \psi_0$. A new collective input is defined as $\hat{u}_{collective} = u_{collective} - mg$ such that the required collective control to hover is already accounted for and $\hat{u}_{collective}$ then specifies up and down movement from the hover position. In near hover conditions, both the gyroscopic effect due to rigid body rotation and the gyroscopic effect caused by changing rotor speeds are negated as they are insignificant relative to the control moment generated by the actuators. Additionally, small terms are are dropped from

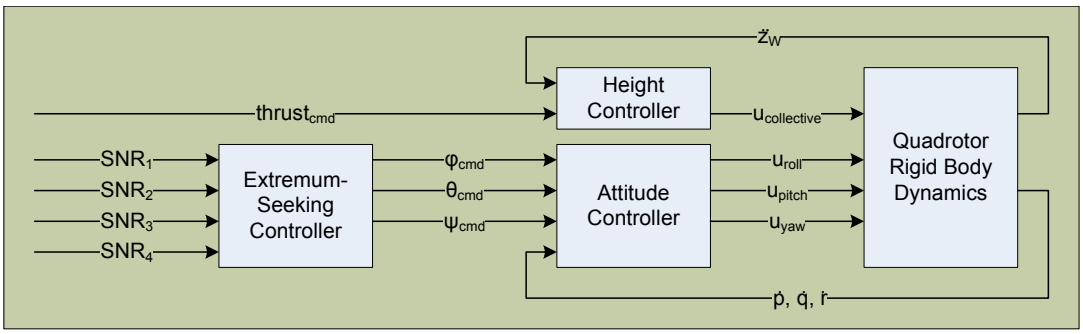

Figure 2.2: Quadrotor control loops.

the x_W and y_W dynamics. The linearized Newton-Euler equations are then as follows.

$$\begin{aligned}
\ddot{x}_W &= g(\phi \sin\psi_0 + \theta \cos\psi_0) \\
\ddot{y}_W &= g(\theta \sin\psi_0 - \phi \cos\psi_0) \\
\ddot{z}_W &= \frac{1}{m}\hat{u}_{collective} \\
\dot{p} &= \frac{L}{I_x}u_{roll} \\
\dot{q} &= \frac{L}{I_y}u_{pitch} \\
\dot{r} &= \frac{1}{I_z}u_{yaw}
\end{aligned} \tag{2.10}$$

Onboard the quadrotor, the attitude controller implements three independent PD control loops, one for each orientation angle [20]. Measurements from the quadrotor's gyroscopes are used as inputs to the controller in addition to the desired angle commands output by the extremum-seeking controller. When the direct thrust input is set to neutral, the height controller serves as an accumulator which attempts to maintain a constant height (i.e., zero acceleration in the z_W axis) based on measurements from the quadrotor's accelerometers. Otherwise, the height controller is simply a pass through for manual thrust control. As the quadrotor's design and controllers allow it to move in any direction, the extremum-seeking controller can thus

treat the quadrotor as a holonomic system in the horizontal plane while the height controller maintains position in the vertical plane.

A position controller can be implemented if an external position system is available (i.e., GPS, motion capture system, etc.). However, since the motivation in this thesis is for a communications relay robot in an unknown indoor environment, it's assumed that such a system is unaccessible. Therefore, the quadrotor will tend to drift due to measurement noise and discrete integration. Collision avoidance sensing via cameras or range finders (ultrasonic or laser) is necessary in order to maintain a safe distance between the quadrotor and any obstacles. The remainder of this thesis discusses the development and implementation of the extremum-seeking controller which includes the collision avoidance algorithm.

Chapter 3

Technical Background

3.1 Antenna Diversity

The primary impairment wireless communications channels are susceptible to is fading — the deviation in interference of a propogating signal. Fading is caused by multipath propogation which is the reception of multiple copies of a signal due to scattering by objects in the RF environment. These signal copies can undergo different attenuations, distortions, delays, and phase shifts, resulting in random fluctuations of the signal level at the receiver. Particularly in NLOS indoor or urban environments, an RF signal can be reflected along multiple paths before finally being received [21, 22].

Fading may occur at specific times, frequencies, or locations. Deep fades occur when the signal degredation is so severe that the signal is unusable, if even detected. The most effective way to combat multipath propogation is with increased transmitter power but this is not always an option due to size, weight, and power limitations. Diversity schemes attempt to improve message reliability without increased power by employing mulitple communications channels in order to combating fading. Fre-

quency diversity sends the same signal on multiple carrier frequencies whereas time diversity sends multiple copies of the signal at different time instances. Space diversity transmits the signal over multiple propogation paths by using multiple transmitting and/or receiving antennas; thus it's also known by the name antenna diversity.

Antenna diversity uses two or more antennas to improve wireless links and is especially effective at mitigating multipath. Multiple antennas provide the advantage that while one receiving antenna may be in a deep fade or experiencing interference, it's probable that another antenna has a sufficient signal. Movements as little as a 1/2 wavelength may be enough to escape a deep fade. The SPAWAR systems discussed in Subsection 1.2.2 didn't employ antenna diversity and were thus subject to premature deployment of relay nodes as local RF nulls were encountered.

3.1.1 Shannon-Hartley Theorem

As messages are passed between radios in a wireless networks, each message received by a radio typically contains a measure of the signal quality called signal-to-noise ratio (SNR), $\frac{S}{N}$. SNR provides an indication of how much a signal has been corrupted by noise. SNR is calculated by

$$\frac{S}{N} = P_{signal} - P_{noise} \tag{3.1}$$

where P_{signal} is the incoming power and P_{noise} is the background noise, both parameters expressed in dB.

The goal of the communications relay is to maximize the channel capacity, C, the theoretical maximum error-free data rate for a communications link. The Shannon-Hartley theorem states that the maximum channel capacity that can be achieved by a given SNR where B is the bandwidth of the channel is given by,

$$C = B \log_2 \left(1 + \frac{S}{N}\right). \tag{3.2}$$

Hence, maximizing the SNR is equivalent to maximizing the channel's throughput. SNR measurements will serve as the input to the communications relay controller which will presented in Chapter 4.

3.2 Extremum-Seeking Control

Extremum-seeking control is an adaptive, model-free strategy for finding an unknown, optimal input to a nonlinear system. It's useful for applications where the nonlinear system behaves as a reference-to-output map — the goal is to maximize the output but the mapping is unknown. The traditional methodology involves probing the system with sinuisoidal inputs (i.e., a dither signal) which in turn creates variations in the output and from these perturbations, the input can thus be tuned in the direction that maximizes the output [23].

The extremum-seeking algorithm is essentially a modified formulation of the well-known gradient descent algorithm (also called steepest descent). Gradient descent is an optimization algorith for finding the local minimum of a function. It's simple computationally and guaranteed to find the minimum through numerous iterations [24]. Typical applications of gradient descent include solving complex integrals or, in signal processing, finding filter coefficients for a least mean square (LMS) filter [25]. Extremum-seeking follows the same gradient descent methodology, but unlike the gradient descent algorithm, the function is unknown.

An extremum-seeking controller attempts to solve the real-time optimization problem

$$\theta^*(t) = \arg\max_{\theta \in R} J(t, \theta) \tag{3.3}$$

where J is an unknown, possibly time-varying, smooth cost function and θ is the input parameter. At the optimal input, θ^*, the first derivative of J equals zero

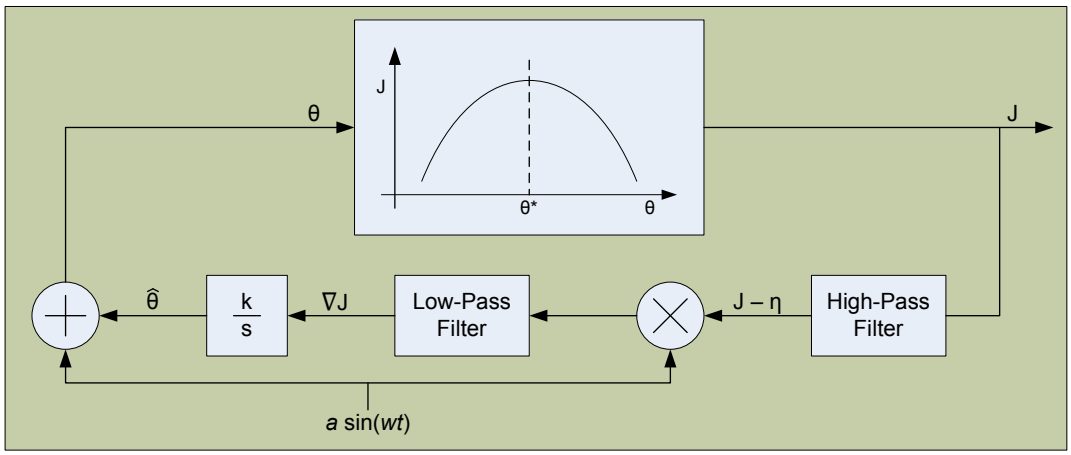

Figure 3.1: Notional extremum seeking controller.

(i.e., $J'(t, \theta^*) = 0$) and the second derivative is less than zero, (i.e., $J''(t, \theta^*) < 0$), indicating a local maximum has been reached.

Figure 3.1 shows a typical extremum-seeking algorithm. The algorithm works by generating a measure of the local gradient of the mapping $J(\theta)$ by injecting a perturbation signal directly into the plant. The perturbation signal is the estimate of the optimal input, $\hat{\theta}$, modulated with a carrier signal, $\alpha \cos(\omega t)$. The plant behaves a static map and produces an output that is also a sinusoidal signal. A high-pass filter removes the DC offset and the signal is then demodulated and low-pass filtered to obtain the gradient estimate, ∇J. The integral of the gradient is then used to update $\hat{\theta}$. See [26, 27] for stability proofs and further details.

3.2.1 Extremum-Seeking Applications

Extremum-seeking controllers have been developed for numerous applications: maximizing biomass production in bioreactors [28]; reducing instabilities and maximizing pressure rise in axial flow compressors in jet engines [29]; formation flight of aircraft

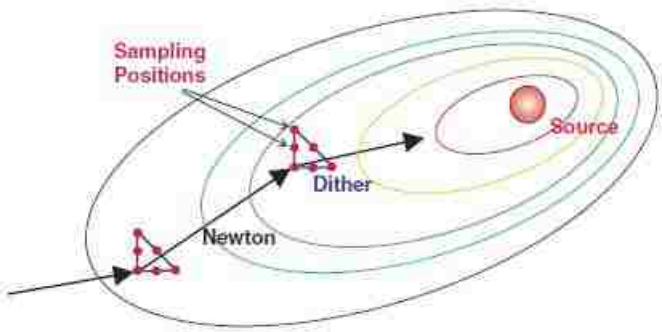

Figure 3.2: Extremum-seeking by robot motion.

[30]; improving a pneumatic anti-lock braking system (ABS) [31]; automatic tuning of proportional-integral-derivative (PID) controller gains [32].

Extremum-seeking was employed in the fixed-wing UAV scenario discussed in Section 1.2. In two-dimensions, the extremum-seeking controller's sinusoidal perturbation appears circular. Instead of a generated sinusoidal input, the UAV orbits around a center-point to produce the cyclic motion. The extremum-seeking controller then updates the position of the center-point based on SNR measurements taken as the UAV flies [33].

Similarly, in [34], a robot performed a sequence of quick motions to serve as the required dither signal. The vehicle stops momentarily at six locations to take sensor measurements as shown in Figure 3.2. The use of six measurements allows estimation of the Hessian matrix and thus Newton's method can be used instead of the standard gradient descent algorithm. The Newton gradient climbing algorithm should, theoretically, converge faster.

Extremum-seeking control was used in [35] to steer a formation of autonomous underwater vehicles (AUVs), specificially a group of Slocum Gliders, shown in Figure 3.3. The AUVs are kept in formation by artificial potential fields. Using GPS,

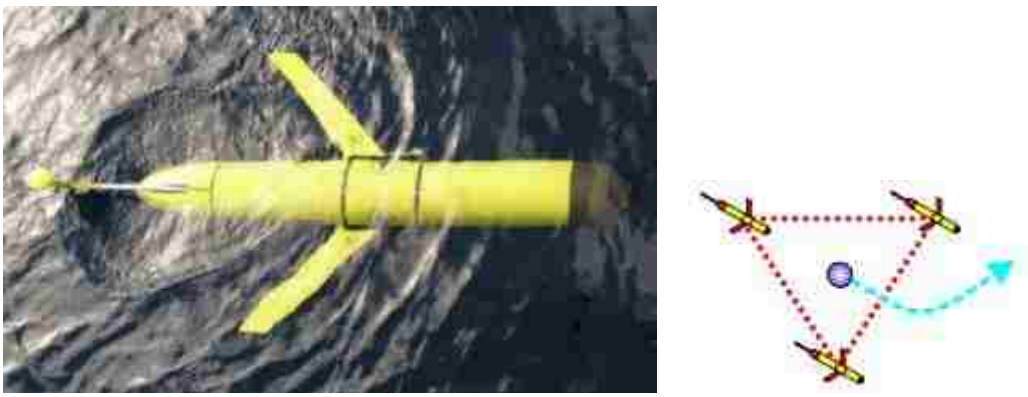

Figure 3.3: Extremum-seeking by multiple AUVs.

the algorithm treats the AUVs as point masses which attract neighboring gliders if they're too far apart and repel them if they're too close. The entire formation then moves as one, following the gradient estimated from sensor measurements obtained from each vehicle (e.g., temperature measurements).

Chapter 4

Extremum-Seeking via Directional Antenna Diversity

4.1 Extremum-Seeking Algorithm

The goal of the extremum seeking controller is to achieve the maximum throughput for the communications channel being relayed by driving the quadrotor to an optimal location in an unknown RF field. Antenna diversity is used to generate the required dither signal for the quadrotor communications relay. The layout of the antennas provides a psuedo circular motion — antennas are located at each of the quadrotor's four rotors as in Figure 4.1 and Figure 4.2. The use of multiple antennas allows the quadrotor to survey the communications field and find the direction to move so that communications are improved.

Directional antennas are used in the proposed antenna diversity scheme because they radiate greater power in a specific direction as opposed to omnidirectional antennas which attempt to radiate power uniformly. This allows the directional antennas to sense the RF environment and hence, direction of improved communications per-

formance. Directional antennas provide additional advantages as well. The authors in [36] showed that when the radiation is focused towards the receiver, directional antennas typically outperform omnidirectional antennas in NLOS indoor environments. Furthermore, omni antennas are prone to introducing interference as well as wasting power.

The algorithm uses antenna selection diversity — the incoming signal is received by all four antennas but only the signal taken from the antenna with the highest SNR is used. A more complex antenna diversity scheme (i.e., multiple output with signal combining [37]) could be implemented, but with directional antennas in use, the benefit would be marginal while the requisite hardware and software would be significantly more complex.

As the quadrotor relays messages between the two end nodes, eight SNR measurements are obtained — two from each of the four antennas. After obtaining the SNR measurements, the first step in the algorithm is to select the two antennas to use for relaying by choosing the antenna with the highest SNR measurement from the four measurements available per node. Using this information, the controller performs two independent tasks simultaneously in order to maximize the channel capacity: (1) maximize the SNR measurements of the two antennas in use, and (2) balance the two SNRs.

4.1.1 Peak-Seeking and Balancing

The peak-seeking and the balancing components of the algorithm can be performed independently because the respective forces they produce will be enacted orthogonal to each other. The balancing force acts upon the line between the two selected antennas whereas the peak-seeking force works in the axis perpendiclar to this line. Given the two antennas selected, there are two possible formulations for the maximiza-

tion component of the algorithm. It's assumed the RF field can be characterized by an unknown smooth function $F(x, y) : \mathbb{R}^2 \to \mathbb{R}$. Thus, if opposing antennas are selected, as in Figure 4.1 where the two antennas along the x-axis are chosen, the peak-seeking gradient, $\nabla F(y)$, can be estimated with the SNR measurements obtained by employing the central finite difference method [38]

$$G_p(y) := \nabla F(y) \approx \frac{F(y + \epsilon e_j) - F(y - \epsilon e_j)}{2\epsilon} \tag{4.1}$$

where ϵ denotes the finite difference dither size and e_j is the jth unit vector. The dither size will be constant as it's the distance between the quadrotor center-point and any of the four antennas located at their respective rotor. For the second case where adjacent antennas are selected, such as in Figure 4.2 where the two antennas along the x'-axis are chosen, a modified version of the central finite difference method is used to estimate $G_p(y')$. The gradients $G_p(y' + \epsilon e_{j'})$ and $G_p(y' - \epsilon e_{j'})$ can be obtained from

$$G_p(y' + \epsilon e_{j'}) = \frac{F(y' + \epsilon e_{j'} + \epsilon e_{i'}) - F(y' + \epsilon e_{j'} - \epsilon e_{i'})}{2\epsilon} \tag{4.2}$$

and

$$G_p(y' - \epsilon e_{j'}) = \frac{F(y' - \epsilon e_{j'} + \epsilon e_{i'}) - F(y' - \epsilon e_{j'} - \epsilon e_{i'})}{2\epsilon} \tag{4.3}$$

where $e_{i'}$ is the i'th unit vector, $e_{j'}$ is the j'th unit vector, ϵ is the finite difference dither size which, due to the symmetry of the quadrotor, is the same in both the i'th and j'th directions. The gradient $G_p(y')$ is then obtained by the mean

$$G_p(y') = \frac{1}{2}(G_p(y' + \epsilon e_{j'}) + G_p(y' - \epsilon e_{j'})). \tag{4.4}$$

To orient the gradient to the body-reference axes, $G_p(y')$ can then be rotated counter-clockwise by the rotation matrix

$$R(45^\circ) = \begin{bmatrix} \cos(45^\circ) & -\sin(45^\circ) \\ \sin(45^\circ) & \cos(45^\circ) \end{bmatrix} \tag{4.5}$$

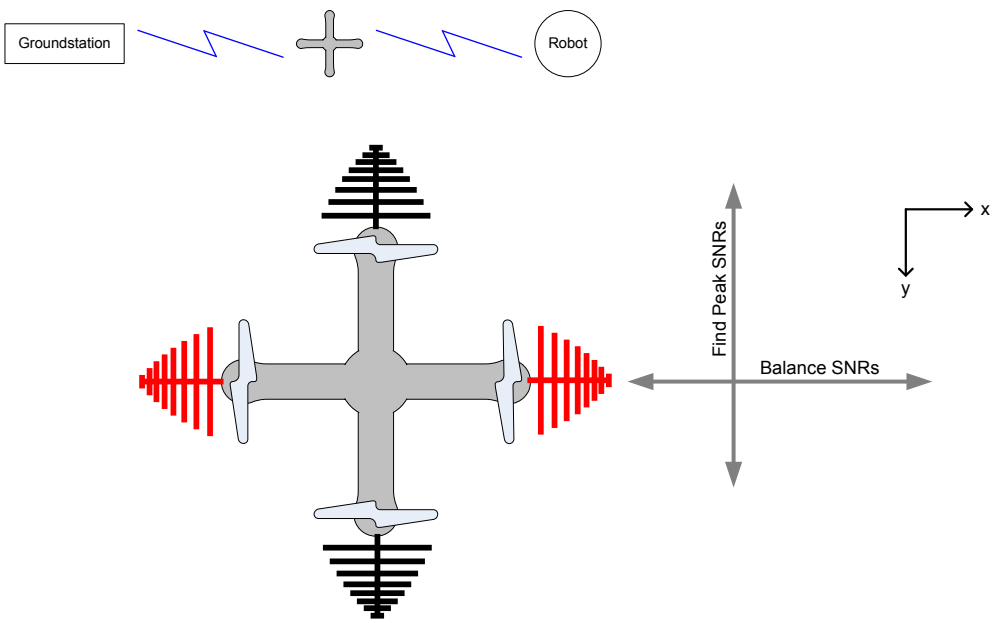

Figure 4.1: Extremum-seeking algorithm — opposing antennas selected.

such that

$$G_p(y) = G_p(y')R(45°). \tag{4.6}$$

The quadrotor can then simply follow the peak-seeking gradient G_p to maximize its received SNR values.

The balancing component of the extremum seeking algorithm is simple in its construction as only the max SNRs of the two antennas in use are needed. If the chosen antennas are opposite, the balancing gradient, $\nabla F(x)$, can be approximated by

$$G_b(x) := \nabla F_b(x) \approx \delta \left| F(x + \epsilon e_i) - F(x - \epsilon e_i) \right| = \delta \left| \frac{S}{N}_{max1} - \frac{S}{N}_{max2} \right| \tag{4.7}$$

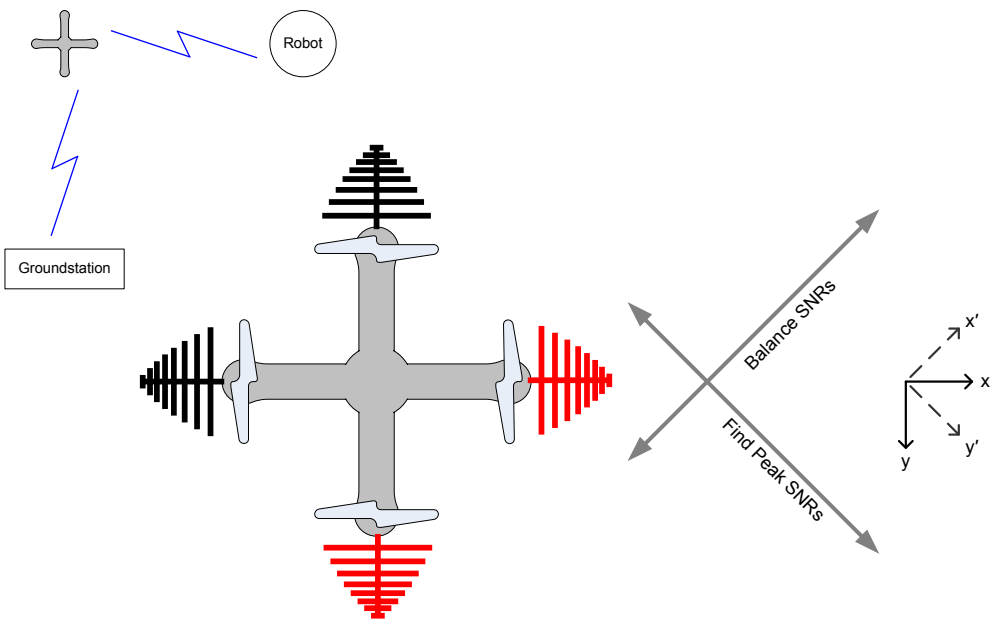

Figure 4.2: Extremum-seeking algorithm — adjacent antennas selected.

or if the chosen antennas are adjacent

$$G_b(x') := \nabla F_b(x') \approx \delta \left| F(x' + \epsilon e_{i'}) - F(x' - \epsilon e_{i'}) \right| = \delta \left| \frac{S}{N}_{max1} - \frac{S}{N}_{max2} \right|$$

$$G_b(x) = G_b(x') R(45^\circ). \tag{4.8}$$

where δ takes the value of 1 or -1 in order to orient the gradient vector appropriately (e.g. in Figure 4.2, if end node 1's strongest antenna is the bottom antenna and end node 2's strongest antenna is the right antenna, δ would equal -1 such that the gradient is oriented along the x'-axis). The quadrotor can then follow the negative of the balancing gradient, $-G_b$, so as to equate the two maximum SNR values.

4.1.2 Collision Avoidance

In order to provide collision avoidance capabilities, an artificial potential field is constructed so as to drive the quadrotor away from any obstacles. In other words,

a force field is created around the vehicle. The artificial potential, $U_{ca}(x)$, depends on the distance, $D(x)$, to the object — if the object is farther away than a specified distance, D^*, then the object is considered to be sufficiently far enough away from the quadrotor and can thus be ignored. In practice, this can be considered as the obstacle being out of the sensor's range. The gradient of the artifical potential field is defined as follows [39].

$$G_{ca}(x) := \nabla U_{ca}(x) = \begin{cases} \left(\frac{D(x)}{||D(x)||^2}\right) & \text{if } D(x) \leq D^* \\ 0 & \text{if } D(x) > D^* \end{cases} \tag{4.9}$$

4.2 Quadrotor Dynamics

As discussed in Section 2.3, the quadrotor can be considered a holonomic kinematic system and is thus treated as a point mass with the position of the vehicle represented in the horizontal plane by $\mathbf{x} \in \mathbb{R}^2$ (*i.e.*, $\mathbf{x} = \begin{bmatrix} x & y \end{bmatrix}$). The quadrotor dynamics can be represented by

$$\dot{\mathbf{x}} = K_p G_p(\mathbf{x}) - K_b G_b(\mathbf{x}) - K_{ca} G_{ca}(\mathbf{x}) \tag{4.10}$$

where the gains K_p and K_b increase/decrease the resultant velocity and scale the rate of convergence of the peak-seeking versus the balancing controllers; K_{ca} is set so as to prevent colliding with obstacles. Appropriate values for the gains were determined by trial and error using the simulations discussed in Section 5.3.

The optimization motion will persist until the quadrotor converges to within the neighbord of a minima (i.e., $G_p(\mathbf{x}) \approx G_b(\mathbf{x}) \approx G_{ca}(\mathbf{x}) \approx 0$). At this point, the SNR measurements of the quadrotor's two communications links will be approximately maximized and balanced. The quadrotor may remain in a hover at this location as long as the SNR of each link remains above a specified threshold, $\frac{S}{N} \geq \frac{S}{N}_{thresh}$. If one or both of the SNRs drop below the threshold (i.e., $\min\left(\frac{S}{N}_{max1}, \frac{S}{N}_{max2}\right) <$

$\frac{S}{N}_{thresh}$), the algorithm will begin anew. The algorithm may converge to a local minimum instead of a global minimum, however, this is not considered a shortfall of the algorithm as its still provides a more optimal motion planning strategy for communications than can be achieved by traditional position-based methods.

Chapter 5

Simulations

5.1 Overview

Simulations of the extremum-seeking controller, developed in MATLAB, are presented in this section. In these simulations, the quadrotor flies in a two-dimensional environment serving as a communications relay between two fixed end nodes (i.e., the groundstation and robot in the scenario presented in Section 1.1). Equipped with a laser, the quadrotor moves autonomously, avoiding obstructions and optimizing the communications links despite the presence of noise sources. Simulations are conducted in varying environments ranging from open outdoor environments to indoor environments with multiple noise emitters in and around a building. Additional simulations demonstrate the potential of expanding the proposed algorithm to multiple quadrotors.

5.2 Simulation Design

The quadrotor communications relay is modeled as per Equation 4.10. Height is neglected as it's assumed to be held constant. The quadrotor travels in a black and white bitmap image where black represents obstacles and white represents freespace. A laser emanates from the quadrotor at every 90°, simulating having a range finder located at each of the four rotors. The simulation looks at all points in the bitmap that are in the path of each laser beam and within the sensor's defined range — a black pixel detected along the path signifies a hit. The distance between the simulated range finder and the detected hit serves as the input to the collision avoidance gradient function, Equation 4.9.

SNR measurements, the inputs for the peak-seeking and balancing gradient functions, are simulated to account for attenuation and interference in an indoor or dense urban environment [40, 41]. Power measurements are calculated by the log-distance path loss model

$$P_{Rx} = P_{Tx} - PL \tag{5.1}$$

where P_{Rx} is the received power and P_{Tx} is the transmitted power, both expressed in dBm. The path loss, PL, is calculated by

$$PL = PL_0 + \gamma 10 \log_{10} \left(\frac{d}{d_0} \right) \tag{5.2}$$

where d is the distance between the transmitter and receiver. The path loss exponent, γ, takes on values ranging from 2 for free space up to 4 for a very noisy, lossy environment. The reference path loss, PL_0, is calculated at a reference distance d_0 by the Friis transmission equation

$$PL_0 = 10 \log_{10} \left(\frac{1}{G_{Tx} G_{Rx}} \left(\frac{4\pi d_0}{\lambda} \right)^2 \right) \tag{5.3}$$

where λ is the wavelength of the transmitted signal. For the antenna gains, G_{Tx} is taken to be unity and G_{Rx} takes on a value ≤ 1 to account for the directivty of the quadrotor's antennas.

The constant noise power is calculated, in dBm, by the addition of the thermal noise power, $P_{thermal}$, and the noise figure, NF.

$$P_{noiseConstant} = P_{thermal} + NF \tag{5.4}$$

Thermal noise is calculated per the Johson-Nyquist formula at room temperature

$$P_{thermal} = -174 + 10\log 10(B) \tag{5.5}$$

where B is the radio's bandwidth. ZigBee radios, discussed in Section 6.2, have a bandwidth of 5 MHz and a noise figure of approximately 2.

Noise sources may be placed throughout the environment, increasing the background noise which in turn decreases the SNR. The power radiating from the center of a noise source, $P_{noiseSource}$, is calculated by a similar log-distance path loss model as Equation 5.1. At each antenna, the summation of the dissipated power from the various noise emitters is then added to the constant noise power such that $P_{noise} = P_{noiseConstant} + \sum P_{noiseSource}$. SNR is calculated for each of the four antennas as per Equation (3.1) with $P_{signal} = P_{Rx}$. The peak-seeking and balancing gradients can then be calculated as discussed in Subsection 4.1.1.

The quadrotor velocity is calculated as per Equation 4.10. In the simulation, the algorithm is executed in discrete time with a stepsize α as follows.

$\mathbf{x}(0) = \mathbf{x}(0)$
$k = 0$
loop
  $G(k) = K_p G_p(\mathbf{x}(k)) - K_b G_b(\mathbf{x}(k)) - K_{ca} G_{ca}(\mathbf{x}(k))$
  if $G(k) > \eta$ **then**

$\mathbf{x}(k+1) = \mathbf{x}(k) + \alpha G(k)$
else
$\mathbf{x}(k+1) = \mathbf{x}(k)$
end if
$k = k + 1$
end loop

If the gradient is sufficiently small (*i.e.*, $G \leq \eta$) then the quadrotor is in the neighborhood of the optimal position and will remain in a hover.

Typical gradient descent algorithms employ a line search to find an optimal step-size in order to minimize the gradient function G. Given the everchanging nature of the communications field and the movement of the end nodes, the quadrotor should be close to an optimal position but does not need not be in the exact perfect position as that position will likely continually change. As discussed in Section 3.1, small movements are often adequate to resolve issues with a communications channel. Thus α is chosen as a fixed-step size so the quadrotor should not move beyond the range of its collision avoidance sensors but shouldn't make such small movements as to require excessive time to execute the algorithm. As will be seen in Chapter 6, the fixed-step size works the same with real hardware — after taking measurements and calculating the gradient, the quadrotor moves for a fixed amount of time before slowing to a hover and taking new measurements.

5.3 Simulation Results

Figure 5.1 shows the case where the quadrotor is in free space, the end nodes have identical communication performance, and there are no obstacles or extraneous noises. Under these conditions, the quadrotor converges to the the position equidis-

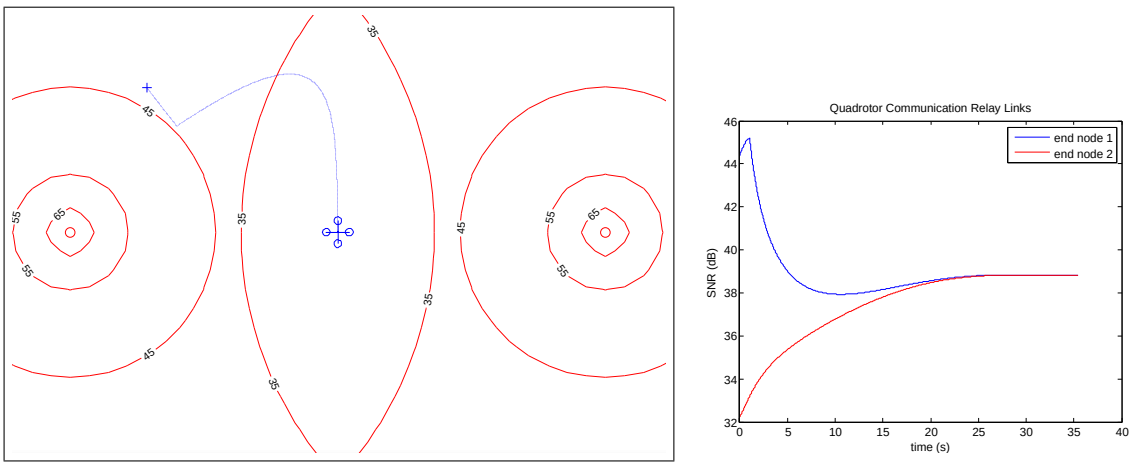

Figure 5.1: Simulation — free space environment.

tant between the two end nodes, as would happen if a position-based algorithm were implemented. The blue cross indicates the quadrotor's starting position with the blue dashed line indicating the quadrotor's path to it's final position. The red concentric circles emanating from the end nodes display the received power at those locals. The accompanying graph shows the SNRs achieved by the two links — the quadrotor movement causes the two links to converge to the maximum achievable throughput in the RF environment.

A localized noise source is added to the environment for the simulation show in Figure 5.2. The interfering noise power is illustrated by green concentric circles originating from the noise source. As is often the case with real RF environments, the optimal location for the communication relay is not the location that would be given by a position-based algorithm. While the throughput of an ideal, noiseless environment such as the previous simulation cannot be achieved, the link SNRs are maximized for the given noisy environment.

In Figure 5.3, the quadrotor is in a complex indoor environment. As discussed in Section 5.2, a simulated laser range finder detects obstacles and allows the quadrotor

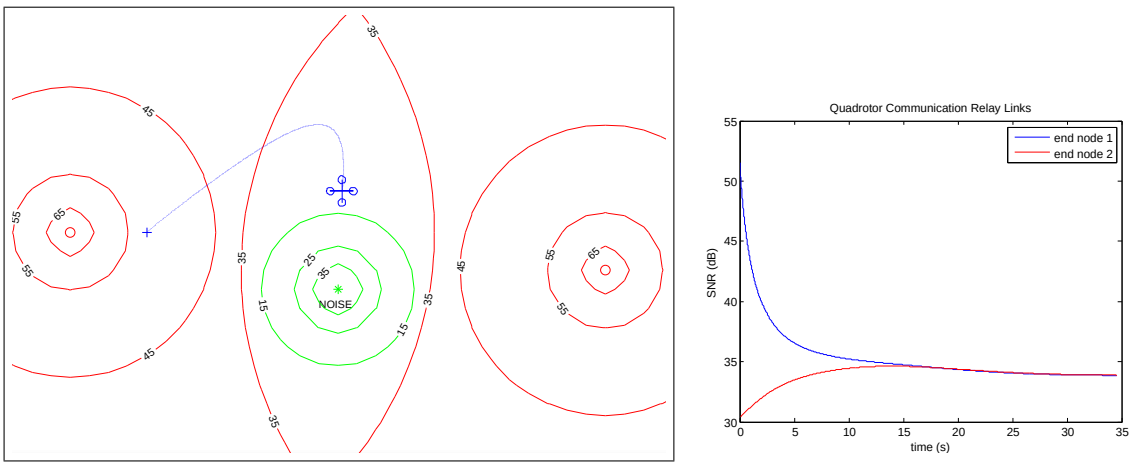

Figure 5.2: Simulation — noise source in environment.

to avoid collisions. The quadrotor moves to the best location possible in the RF field while still maintaining seperation from the walls. While the quadrotor is able to achieve a minima, the graph shows that, due to the presence of obstacles, the algorithm is able to approximately but not perfectly balance the SNRs of the two end nodes.

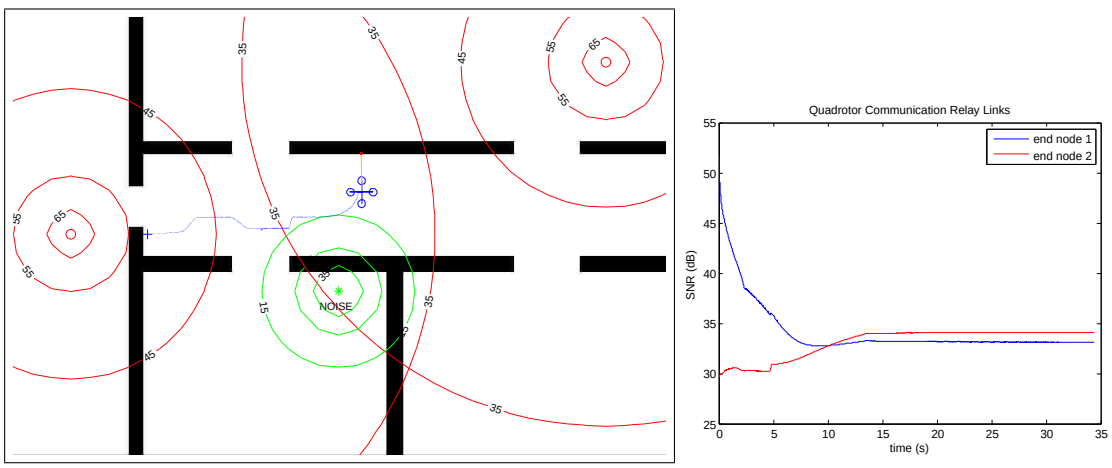

Figure 5.3: Simulation — noise source and obstacles in environment.

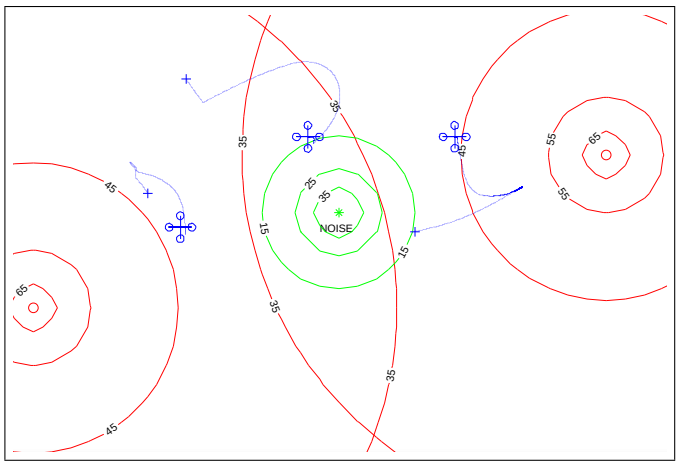

Figure 5.4: Simulation — three quadrotors in free space.

While the focus has been on a single quadrotor, the algorithm can be extended to work with multiple quadrotors. Figure 5.4 shows three quadrotors now forming a communications chain. Section 7.2 discusses some of the issues that need to be addressed in order to effectively implement the algorithm with more than one communications relay in the loop.

Chapter 6

Experimental Results

6.1 Goals

Experiments with hardware have been conducted to prove the viability of using antenna diversity to source the proposed extremum-seeking controller. In these experiments, the quadrotor is electronically leashed to a telemetry station. The two systems communicate periodically with eachother with the quadrotor taking SNR measurements as messages are received. The goals of the experiments were to [1] characterize and demonstrate the ability of the antennas to produce a sufficient control input, and [2] and demonstrate the algorithm in action, with real hardware.

6.2 Hardware

The AscTec Hummingbird quadrotor from Ascending Technologies GmbH [42, 20] serves as the platform for these experiments. The Hummingbird is small enough to fly indoors (wingspan of 55cm, height of 8cm, weight of 500g with a battery), yet

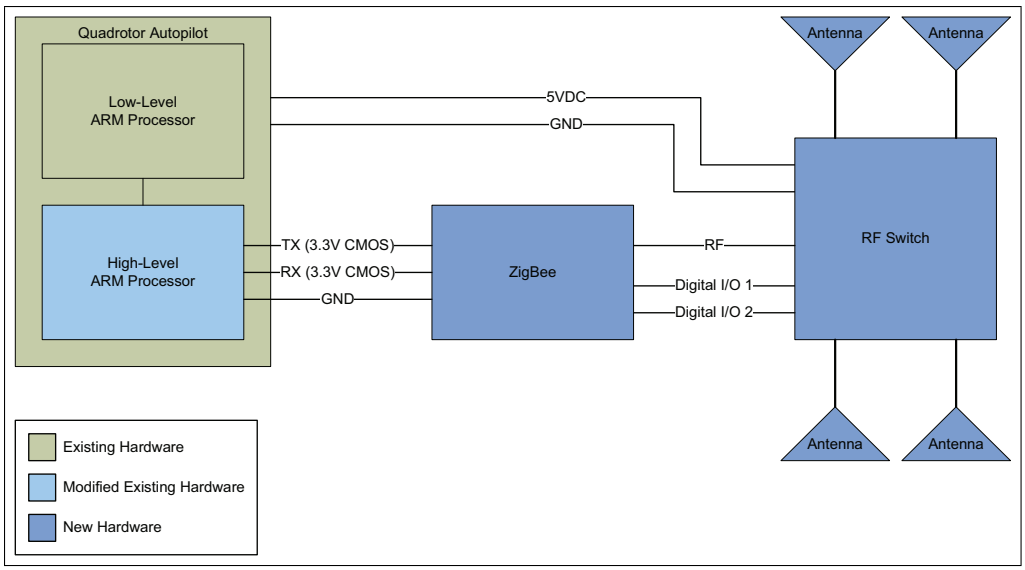

Figure 6.1: Quadrotor architecture.

versatile enough to fly for 20+ minutes with a 200g payload. The quadrotor is also durable enough to survive most crashes — the rotor blades are made of soft, flexible plastic which will not damage anything the Hummingbird may run into and allows for easy repair.

As discussed in Section 2.3, the Hummingbird's low-level flight controls are taken care of by the attitude and height controllers running at a 1kHz update rate on an ARM processor (see Figure 6.1. A second ARM microcontroller executes the higher-level extremum-seeking controller code which is discussed in the ensuing section detailing the experimental software.

ZigBee transceivers are used as the communications link between the Hummingbird and the telemetry station. The radios were chosen for their small size, low cost, and low power. Additionally, the chosen Digi XBee 802.15.4 OEM RF modules have digital I/O which is used for controlling the RF switch. Onboard the quadrotor, an XBee radio is attached to a UART on the high-level ARM processor with the cor-

Figure 6.2: Hardware — AscTec Hummingbird quadrotor.

responding XBee radio attached the telemetry monitor via USB. While the ZigBee radios can be used as a transparent serial channel, for these experiments, the radios are used in application programming interface (API) mode. This allows the digital I/O states to be changed quickly and provides access to detailed packet information, specifically signal strength measurements as will be discussed in Section 6.3.

A single-pole four-throw RF switch connects the quadrotor's radio to one of its four antennas at a time. The RF switch is controlled by two TTL voltage level inputs which are driven from the ZigBee radio's digital outputs.

While the desire is to have a true spatial antenna diversity system (see discussion in Chapter 7), due to cost considerations and hardware availability, the RF switch

Figure 6.3: Hardware — XBee ZigBee RF module.

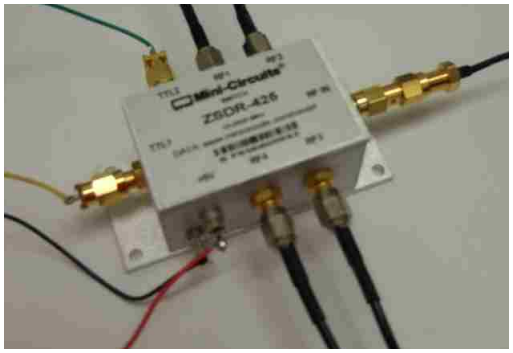

Figure 6.4: Hardware — RF switch.

serves as an ample substitute. The quadrotor's radio transceiver will be able to connect to one of the four directional antennas at a time. Although only one antenna is connected to the radio at a time with this hardware implementation, the measurements can be obtained rather quickly by switching between received packets; the switch can change antennas in about two microseconds. For these experiments, the same data is sent in every packet so as to remove that as a variable. Cycling through all four antennas allows SNR measurements to be obtained for each antenna which are then used as inputs into the extremum-seeking controller.

Two types of antennas, patch antennas and log-perioidic ('logi') antennas, were

Figure 6.5: Hardware — patch antenna.

Figure 6.6: Hardware — log-periodic antenna.

considered for the flight experiments — antenna test results are presented in Section 6.4. The antennas were chosen for use on the quadrotor because of their light weight and highly directional gain pattern. The patch antennas were built by hand from sheet metal while the logi antennas are off-the-shelf printed circuit board (PCB) construction.

A PC running custom telemetry software serves as the ground node to which the quadrotor is tethered via the ZigBee radios. As is typically the case on UGVs, human personnel, and other communication end nodes, the telemetry monitor's ZigBee radio has an omnidirectional antenna. For these experiments, the telemetry monitor is moved around so as to simulate an end node and demonstrate the tethering abilities

Figure 6.7: Hardware — ground station.

of the quadrotor communications relay.

6.3 Software

The quadrotor code for executing the control loops and for sending and receiving messages to/from the telemetry monitor is written in C. The communications code was originally written on a Linux box for ease of troubleshooting and for the purposes of running the antenna tests discussed in Section 6.4 before porting the code to the ARM processor. The telemetry monitor software is written in Processing — an open source data visualization programming language based on Java.

The extremum-seeking algorithm is implemented by passing messages from the telemetry monitor to the quadrotor and vice-versa. Contained in each received message is a received signal strength (RSS) value, a measurement of the power of received

signal. It's assumed that the noise floor is constant over the hardware and RSS is then just an additive constant difference from SNR. Hence, maximizing RSS is equivalent to maximizing SNR.

The telemetry monitor software constructs and transmits XBee API frames periodically to the quadrotor (i.e., pseudo data from an end node). Once a full packet is received by the quadrotor, the RSS measurement is parsed from the packet and stored. If a packet fails the checksum or is not received within a specified time period, the worst-case RSS (i.e., lowest value) is assumed for that antenna. XBee API AT Commands (Hayes command set) are sent from the quadrotor to its ZigBee radio to change the digital out state on the RF switch control lines, thereby switching to the next antenna. Subsequently, an XBee API frame containing telemetry information is downlinked to the telemetry monitor. Packets are parsed as they're received from the quadrotor and the telemetry monitor application then displays the data including the current status of the extremum-seeking algorithm, the current RSS measurements for each antenna, and the resultant gradient vector.

After cycling through all four antennas, if the maximum RSS is greater than a defined threshold, the quadrotor remains in a hover at its current position with its strongest antenna continuing to communicate with the ground node. This state persists as long the chosen antenna remains above the threshold. If the maximum RSS is less than the threshold, the central difference gradient can be calculated per Equation 4.1 using the four RSS measurements. The resultant gradient vector provides the direction of travel which maximizes the RSS and hence, the throughput of the communications link.

On the ARM processor, a lookup table is used to translate the gradient vector into corresponding roll and pitch commands for the Hummingbird. The quadrotor will move autonomously in one of eight directions so as to maximize the RSS of strongest antenna. The roll and pitch commands and the duration of the movements

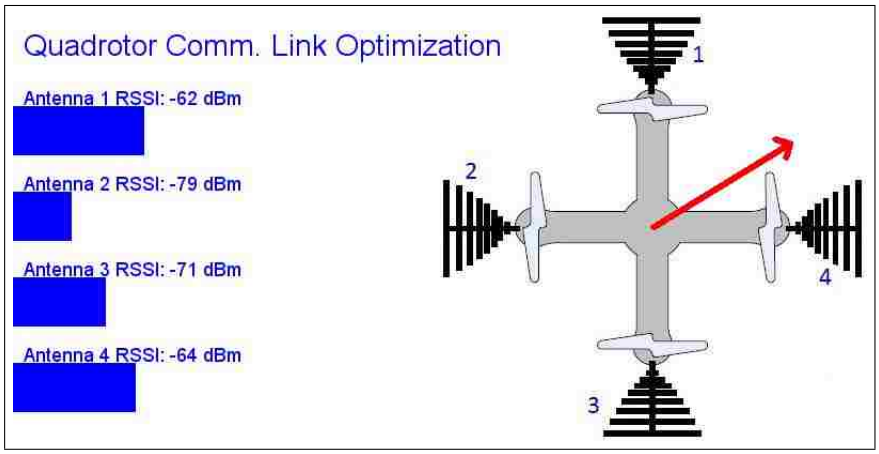

Figure 6.8: Software — telemetry monitor application.

were determined in MATLAB simulations using the model developed in Section 2.2 and refined in experimentation in order to prevent the quadrotor from moving too quickly or too far and colliding into obstacles are becoming unstable.

6.4 Antenna Tests

The purpose of the antenna tests were to demonstrate that the antennas and the RSS values obtained from received messages provided a suitable input to the extremum-seeking algorithm and that the antenna diversity control concept is indeed viable. In order to produce an acceptable input control, it's necessary for the antennas to have virtually identical performance to each other. Secondly, the antennas should be directional enough so as to have significantly stronger RSS when pointed towards the receiver as opposed to when pointed away.

Each patch and log-periodic antenna were tested by looking at the RSS values for each antenna individually. As discussed in Section 6.3, the Linux box served as a

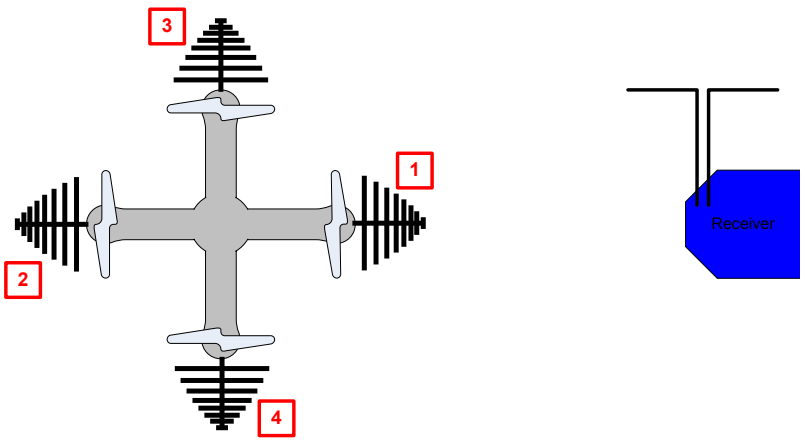

Figure 6.9: Quadrotor orientation for antenna tests.

surrogate quadrotor. For these experiments, the RF switch was not used as instead the antennas were directly connected to the ZigBee transceiver. The antennas were situated at a set distance from the ground station's omnidirectional antenna. Testing was conducted indoors with an attenuator placed on the transmitting antenna. Time-averaged measurements were taken at 90° orientations with the antenna facing towards and away from the telemetry monitor and perpendicular to each side as shown in Figure 6.9.

Tables 6.1 and 6.2 show the results for the patch antenna and logi antenna tests, respectively. Both antennas met the design objectives as the antennas showed relatively consistant performance and directivity. Informal observations showed the patch antenna to be marginally more efficient. This comes at a cost, though, as the patch antennas are considerably larger than the logi antennas and thus, more difficult to integrate into the quadrotor in a usable and neat manner. Antenna improvement options will be discussed in Chapter 7.

Table 6.1: Patch antenna performance.

	Orientation			
	1	2	3	4
Antenna 1 RSS	-51 dBm	-67 dBm	-64 dBm	-60 dBm
Antenna 2 RSS	-52 dBm	-60 dBm	-67 dBm	-63 dBm
Antenna 3 RSS	-50 dBm	-63 dBm	-60 dBm	-59 dBm
Antenna 4 RSS	-50 dBm	-66 dBm	-62 dBm	-63 dBm

Table 6.2: Logi antenna performance.

	Orientation			
	1	2	3	4
Antenna 1 RSS	-54 dBm	-68 dBm	-69 dBm	-67 dBm
Antenna 2 RSS	-56 dBm	-69 dBm	-68 dBm	-67 dBm
Antenna 3 RSS	-53 dBm	-67 dBm	-64 dBm	-64 dBm
Antenna 4 RSS	-50 dBm	-66 dBm	-63 dBm	-66 dBm

6.5 Flight Tests

Initial flights were conducted indoors on a tether system. For the first flights, all the actual hardware was installed onboard the quadrotor but the communications were still being controlled by the Linux box as shown in Figure 6.10. These tests demonstrated that, first of all, the quadrotor could fly even with the additional weight of the antennas, radios, RF switch, and cabling. Secondly, they showed that the additions of the RF switch and the quadrotor's electronics and motors didn't seemingly affect the communications capabilities.

Additional indoor flight test were to be performed with the Hummingbird's processors now in control instead of the Linux box. The use of the tether allowed experimentation, development of vehicle controls (e.g., the lookup table discussed in Section 6.3), and refinement of communications parameters (e.g., when to switch

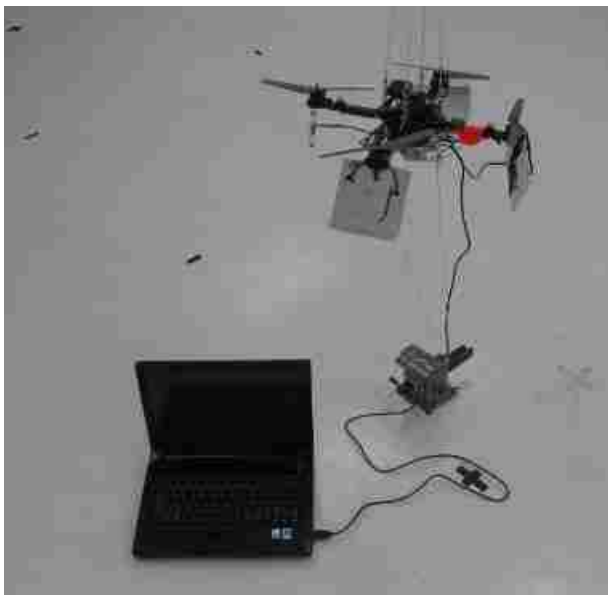

Figure 6.10: Antenna test setup.

antennas and how much time to allow) without the risk of crashing the quadrotor. Outdoor flight tests were to be conducted with the Hummingbird so as to see the extremum-seeking algorithm autonomously flying the UAV. The intended scenario was to have the quadrotor wirelessly tethered to the ground station. The ground station would be mobile — either handheld and moved by a human operator or, as depicted in Figure 6.11, be attached to a ground robot. As the operator or UGV moves away from the quadrotor, the RSS of the antenna in use would fall below the defined threshold. The extremum-seeking algorithm would then commence, causing the quadrotor to fly autonomously to improve the communications link and continuing this method until an acceptable RSS is achieved. Unfortunately, due to time restrictions and asset availability, these last experiments were not realized.

As the simulations demonstrated that the alogirthm itself is viable, the flight tests presented here showed that the extremum-seeking controller can be practically

Figure 6.11: Flight tests.

implemented with real hardware and software. The next chapter, Chapter 7, discusses the next steps that are necessary to implement a fully capable, autonomous quadrotor communications relay.

Chapter 7

Conclusions

7.1 Accomplishments

This thesis presented a quadrotor serving as a communications relay using a novel motion planning algorithm consisting of an extremum-seeking controller for optimizing the communications chain combined with collision avoidance provided by artificial potential fields. The goal of the algorithm is to maximize throughput which is achieved by maximizing the SNR of the two communications links for which the quadrotor is serving as a relay. The input to the controller is based on antenna diversity where multiple antennas receive incoming signals and each antenna can then provide SNR measurements of the RF environment. Based on these measurements, the quadrotor will utilize the best peforming antennas and fly autonomously so as to optimize the communications chain. Simulations as well as flight tests with real hardware were conducted to prove the feasibility of the method.

7.2 Future Work

The ideal communications relay should operate without user intervention or even knowledge — it should be a hybrid system that switches in and out of operation as necessary (i.e., use the direct link between two end nodes when link quality is sufficient and then switch in the relay when necessary), should optimize the communication link, and should perform recovery autonomously (i.e., return to base station, mobile robot, etc.). The optimization goal can be achieved by the motion planning algorithm presented within this thesis, but this is just the first step is designing a viable quadrotor communications relay.

If this work is continued, the immediate focus would be on (1) flying the quadrotor indoors, and (2) improving the communications hardware implementation.

7.2.1 Quadrotor Improvements

To achieve indoor flight, the addition of collision avoidance sensors as well as an improved altitude hold controller is necessary. Infrared proximity sensors mounted at each rotor or a single laser range finder mounted at the center of the quadrotor would be sufficient for collision avoidance. A controller using a simple downward-pointing ultrasonic range finder would provide a significant improvement over the current altitude hold controller which relies on the vehicle's vertically-mounted accelerometer and drifts considerably.

A shortcoming of the quadrotor communications relay is its limited operation time (approximately 20 minutes). Battery life can be extended by reducing weight, which will be required anyways with the addition of the collision avoidance and height sensors. The quadrotor should be customized or redesigned to remove unnecessary components (e.g., GPS antenna and receiver) and lighten excessively heavy

components (e.g., RF switch). Another potential solution that should be investigated is to add perch and stare capabilities to the quadrotor. In a perch and stare scenario, the UAV, after optimizing it's position, could simply land, power down it's motors and other unneeded components, and remaining on the ground serving as a communications relay and conserving battery power.

Finally, additional work is ongoing currently to replace the quadrotor's simple linear control loops with better performing multivariable and/or nonlinear controllers.

7.2.2 Communications Hardware Improvements

For the quadrotor to truly function as a communications relay instead of the tethered system presented in the experiments, suitable hardware must be actualized. The first step to be taken in order to improve the communications system is to replace the RF switch used in the hardware experimentation with a true multi-output antenna selection system. Experiments could then be conducted with a true antenna diversity system instead of the present pseudo antenna diversity system which features a bit of time diversity. Additionally, as most robots and ground stations employ omnidirectional antennas, research will be required to determine the best method for transmitting data from the communications relay (i.e., from one antenna or simultaneously from all four (multi-input)). While multiple transmitters are frequently employed in antenna diversity schemes in order to combat multipath fading, if the receiver is not specifically designed for the reception of multiple copies of the signal, as would be the case with most off-the-shelf robot systems, multipath fading may actually be worsened.

Furthermore, analysis and testing will be required to determine a suitable solution for relaying data between the two end nodes. Can a single radio exchange data between two communication's links in an adequate manner or is a two radio solution

(i.e., one radio for each communications link) preferable and/or required?

7.3 Publications

The work presented in this thesis has been published in the 2010 Proceedings of SPIE Defense, Security, and Sensing [43] and is to be published in an upcoming issue of the Journal of Defense Modeling and Simulation [44].

Bibliography

[1] M. Bruch, R. Laird, and H. Everett, "Challenges for deploying man-portable robots into hostile environments," in *Proceedings of SPIE, Mobile Robots XV and Telemanipulator and Telepresence Technologies VII*, November 2000.

[2] "irobot boeing small unmanned ground vehicle (sugv)," `http://www.sugv.com`.

[3] D. K. Goldenberg, J. Lin, A. S. Morse, B. E. Rosen, and Y. R. Yang, "Towards mobility as a network control primitive," in *5th ACM International Symposium on Mobile Ad Hoc Networking and Computing (MobiHoc)*, Roppongi, Japan, May 2004, pp. 163–174.

[4] D. Carr, "Communications relay grows with expansions of uav missions," Defense Systems, August 2009, `http://defensesystems.com/articles/2009/07/29/c4isr-1-uav-relay.aspx`.

[5] T. Schouwenaars, "Safe trajectory planning of autonomous vehicles," Ph.D. dissertation, Massachusetts Institute of Technology, February 2006.

[6] O. Burdakov, P. Doherty, K. Holmberg, J. Kvarnström, and P.-M. Olsson, "Positioning unmanned aerial vehicles as communication relays for surveillance tasks," in *Robotics: Science and Systems*, Seattle, WA, June 2006.

[7] C. Dixon, E. W. Frew, and B. Argrow, "Electronic leashing of an unmanned aircraft to a radio source," in *44th IEEE Conference on Decision and Control*, Seville, Spain, December 2005.

[8] C. Dixon and E. W. Frew, "Controlling the mobility of network nodes using decentralized extremum seeking," in *45th IEEE Conference on Decision and Control*, San Diego, CA, December 2006.

[9] S. Gil, M. Schwager, B. Julian, and D. Rus, "Optimizing communication in air-ground robot networks using decentralized control," in *2010 IEEE International*

Conference on Robot Communication and Automation (ICRA), Anchorage, AK, May 2010.

[10] "Baa 07-46 landroids broad agency announcement (baa) for information processing technology office (ipto) defense advanced research projects agency (darpa," `http://www.darpa.mil/ipto/programs/ld/ld.asp`.

[11] H. Nguyen, H. Everett, N. Manouk, and A. Verma, "Autonomous mobile communication relays," in *SPIE AeroSense/Unmanned Ground Vehicle Technology IV*, Orlando, FL, April 2002.

[12] H. Nguyen, N. Pezeshkian, A. Gupta, and N. Farrington, "Maintaining communication link for a robot operating in a hazardous environment," in *ANS 10th International Conference on Robotics and Remote Systems for Hazardous Environments*, Gainesville, FL, March 2004.

[13] H. Nguyen, N. Pezeshkian, A. Burmeister, K. Holz, and A. Hart, "Automatic payload deployment system," in *SPIE Unmanned Systems Technology XII*, Orlando, FL, April 2010.

[14] ——, "A modular design approach for the automatic payload deployment system," in *AUVSI's Unmanned Systems North America*, Denver, CO, August 2010.

[15] A. Saleh and R. Valenzuela, "A statistical model for indoor multipath propogation," in *IEEE Journal on Selected Areas in Communications*, February 1987.

[16] N. Michael, D. Mellinger, Q. Lindsey, and V. Kumar, "The grasp multiple micro-uav test bed," in *IEE Robotics and Automation Magazine*, September 2010.

[17] J. How, B. Bethke, A. Frank, D. Dale, and J. Vian, "Real-time indoor autonomous vehicle test environment," in *IEEE Control Systems Magazine*, April 2008.

[18] S. Bouabdallah, P. Murrieri, and R. Siegwart, "Design and control of an indoor micro quadrotor," in *IEEE Inernational Conference on Robotics an Automation*, New Orleans, April 2004.

[19] T. Yechout, S. Morris, D. Bossert, and W. Hallgren, *Introduction to Aircraft Flight Mechanics*. AIAA, May 2003.

[20] D. Gurdan, J. Stumpf, M. Achtelik, K. Doth, G. Hirzinger, and D. Rus, "Energy-efficient autonomous four-rotor flying robot controlled at 1khz," in *The 2006 International Conference on Robotics and Automation*, September 2006.

[21] A. Molisch and M. Win, "Mimo systems with antenna selection - an overview," March 2004.

[22] N. Srivastava, "Diversity schemes for wireless communications - a short review," in *Journal of Theoretical and Applied Information Technology*, May 2010.

[23] M. Krstíc and K. Ariyur, *Real-Time Optimization by Extremum-Seeking Control*. Wiley, October 2003.

[24] X. Wang, "Method of steepest descent and its applications," November 2008.

[25] S. Vaseghi, *Advanced Digital Signal Processing and Noise Reduction*. Wiley, January 2006.

[26] M. Krstíc and H.-H. Wang, "Stability of extremum seeking feedback for general nonlinear dynamic systems," in *Automatica*, April 2000.

[27] M. Krstíc, "Performance improvement and limitations in extremum seeking control," in *Systems and Control Letters*, April 2000.

[28] M. Krstíc, H.-H. Wang, and G. Bastin, "Optimizing bioreactors by extremum seeking," in *International Journal of Adaptive Control Signal Processing*, December 1999.

[29] M. Krstíc, H.-H. Wang, and S. Yeung, "Performance improvement and limitations in extremum seeking control," in *IEEE Transactions on Control System Technology*, March 2000.

[30] M. Krstíc, P. Binetti, K. Ariyur, and F. Bernelli, "Control of formation flight via extremum seeking," in *Proceedings of the American Control Conference*, June 2001.

[31] H. Yu and U. Ozguner, "Extremum-seeking control strategy for abs system with time delay," in *Proceedings of the American Control Conference*, May 2002.

[32] M. Krstíc and N. Killingsworth, "Pid tuning using extremum seeking," in *IEEE Control Systems Magazine*, February 2006.

[33] C. Dixon and E. W. Frew, "Maintaining optimal communication chains in robotic sensor networks using mobility control," in *First International Conference on Robot Communication and Coordination (ROBOCOMM)*, Athens, Greece, October 2007.

[34] E. Biyik and M. Arcak, "Gradient climbing in formation via extremum-seeking and passivity-based coordination rules," in *Asian Journal of Control*, vol. 10, no. 2, 2008, pp. 201–211.

[35] E. Fiorelli, P. Bhatta, and N. E. Leonard, "Adaptive sampling using feedback control of an autonomous underwater glider fleet," in *13th International Symposium on Unmanned Untethered Submersible Tech*, 2003.

[36] A. A. Sani, L. Zhong, and A. Sabharwal, "Directional antenna diversity for mobile devices: Characterization and solutions," in *MobiCom '10*, September 2010.

[37] R. Deepa, K. Baskaran, P. Unnikrishnan, and A. Kumar, "Study of spatial diversity schemes in multiple antenna systems," in *Journal of Theoretical and Applied Information Technology*, May 2009.

[38] J. Nocedal and S. Wright, *Numerical Optimization*. Springer, July 2006.

[39] H. Choset, K. M. Lynch, S. Hutchinson, G. A. Kantor, W. Burgard, L. E. Kavraki, and S. Thrun, *Principles of Robot Motion: Theory, Algorithms, and Implementations*. MIT Press, June 2005.

[40] T. Rappaport, *Wireless Communications: Principles and Practice*. Prentice Hall, January 2002.

[41] J. Seybold, *Introduction to RF Propogation*. Wiley, September 2005.

[42] "Ascending technologies gmbh," `http://www.asctec.de`.

[43] B. Griffin, R. Fierro, and I. Palunko, "Control of an indoor autonomous mobile communications relay via antenna diversity," in *Proceedings of SPIE Defense, Security, and Sensing*, vol. 7692, no. 32, Orlando, FL, April 2010.

[44] ——, "An autonomous communications relay in gps-denied environments via antenna diversity," in *Journal of Defense Modeling and Simulation (JDMS)*, 2011.